Modeling, Control, and Seamless Transition of the Bidirectional Battery-Driven Switched Reluctance Motor/Generator Drive Based on Integrated Multiport Power Converter for Electric Vehicle Applications

Fan Yi, *Student Member, IEEE*, and Wen Cai, *Student Member, IEEE*

***Abstract*—This paper proposes a generalized control method for battery-driven switched reluctance motor (SRM) drives based on integrated multiport power converter (IMPC) with small-ripple bidirectional power flow ability in electric vehicles. Large power ripple caused by the current commutation is a challenge issue for SRM drives, which would lower the system efficiency, requires extra heat dissipation in the battery and shortens its lifetime. The detailed model of the SRM drive and IMPC is developed which covers both motoring and generating modes of operation. Based on this model, an advanced multiobjective power flow control method with repetitive controller is proposed to restrain battery current ripple. Because of the unified model, a seamless transition between various modes can also be achieved. Finally, simulation and experimental results demonstrate the feasibility and superior performance of the proposed control method.**

***Index Terms*—Capacitance reduction, electric vehicle (EV), motor drive, multiport converter, repetitive control, seamless transition, switched reluctance motor, three-port converter.**

I. Introduction

SWITCHED reluctance motor (SRM) [1], [2] has several advantages when compared to other competing machines including but not limited to low cost, fault tolerance, wide range of speed, and ability to operate under harsh environment [3]. Their rotor construction is robust and as well as simple which makes SRMs a serious contender for propulsion systems in electric vehicles (EVs) [4]–[6], including hybrid EVs (HEVs), plug-in hybrid EVs (PHEVs), and battery EVs (BEVs). However, during the period of current commutation between various phases, there exists significant energy transfer between the dc source and the machine, which would lead to large current ripple in the dc source. However, in EVs, the dc source would often consist of Lithium-ion (Li-ion) battery packs because of its high power and energy density. Such large ripple current required by the SRM would cause several problems: 1) excessive temperature rise occurs in the battery pack which leads to bigger cooling system and even thermal management requirement, 2) capacity fading resulted from the excessive temperature rise [7], and 3) pulse charging and pulse discharging is reported to be detrimental to Li-ion batteries' performance [8]. The latter affects the accuracy of battery monitoring and management [9], which might further run to battery's safety issue [10]. As a result, the cost and size of the battery pack and thermal management usually form a major part of the overall system. Conventionally, large electrolytic capacitors are used to restrain this undesirable ripple power, however, the theoretical lifetime of electrolytic capacitances is much shorter than the lifetime of semiconductors and other passive components [11], [12]. Moreover, the SRM allows for bidirectional power flow which means that it can operate in both motoring and regenerative braking modes. This can help to extend the driving range of vehicles by harvesting and transferring kinetic energy into the batteries during the braking period. Therefore, it is important to engineer a seamless and flexible power flow control in SRM drive as used in EV/HEV applications [13].

Recently, many researches have been launched in various fields to adopt either passive compensation approaches or active methods to cancel the undesirable power ripple for batteries in place of large electrolytic capacitors. The current ripple generation and propagation in fuel-cell power system are analyzed and a dual-loop control method to reduce the current ripple through the fuel cell is proposed in [14]. Itoh and Hayashi [15] have added an LC branch at the midpoint of the transformer primary winding and provided ripple control using a small dc capacitor. In reference to renewable energy applications, an extra circuit is utilized to replace the electrolytic capacitors in [16] and [17] to achieve power decoupling with small capacitance requirement. Furthermore, Rong-Jong and Chun-Yu applied coupled inductors into several topologies including H-bridge inverter, bidirectional dc–dc converter, and bidirectional H-bridge converter, to serve as main topology for injecting harmonic current into the dc bus [18]. Furthermore, several new topologies are presented as inverter and rectifier with power decoupling capability to cancel the power ripple in [19] and [20] for power system and microgrid applications. In [21], previous method are summarized and the idea of using three-port converter to achieve capacitance minimization for sing-phase inverter and rectifier is proposed. Despite of the feasibility of all these methods, they mainly focus on fixed-frequency (double-utility frequency, 100/120 Hz) power ripple reduction.

In case of the battery-driven SRM drive system, several specific attributes are worth noticing. First, following the motor

Manuscript received July 30, 2015; revised October 26, 2015; accepted December 3, 2015. Date of publication December 17, 2015; date of current version May 20, 2016. Recommended for publication by Associate Editor M. Ferdowsi.

The authors are with the Renewable Energy and Vehicular Technology Laboratory, Department of Electrical Engineering, University of Texas at Dallas, Richardson, TX 75080 USA (e-mail: fan.yi@utdallas.edu; caiwen600@gmail.com).

Color versions of one or more of the figures in this paper are available online at http://ieeexplore.ieee.org.

Digital Object Identifier 10.1109/TPEL.2015.2510286

speed, the frequency of power ripple in the SRM system would vary (i.e., various power ripple frequencies will be taken from the battery). Second, the power mismatch during current commutation period is nonlinear and uncertain which will generate multiple harmonics instead of only double-utility frequency power ripple. Hence, it is more difficult to deal with such unbalanced power with small capacitors. The method based on commutation elimination is discussed in [22] to overcome the disadvantages of high dc-link capacitance requirement. Based on the idea of modifying the turn-off and turn-on procedure, a direct dc-link voltage control scheme was developed in [23] and [24]. Similarly, Suppharangsan and Wang proposed a modified switching technique to replace hysteresis control for dc-link capacitor minimization and verified its feasibility in [25]. However, the current rating for switches and diodes would increase. By employing various torque ripple reduction method, including both machine design [26], [27] and control strategies [28]–[31], the power ripple can also be reduced. However, the extent to which this can be achieved is always limited by the efficiency of the motor [32]. In [33], split dc-link capacitor technology is presented to reduce the dc-link capacitance requirement under the precondition of balanced energy consumption between two capacitors.

A new integrated multiport power converter (IMPC) has been proposed and analyzed for SRM drives in [34], which can achieve dc-source current ripple reduction with fewer switches and capacitors. These advantages of IMPC make it potential for EVs with battery packs. However, Cai and Yi [34] discuss the capacitance requirement and the operation principle of IMPC. Control strategy and bidirectional power flow are not introduced. Using IMPC as the main SRM drive topology, this paper develops the model of the overall system incorporating SRM and IMPC. Both motoring and regenerating modes can be described using this model. Consequently, a new control method is proposed to achieve battery current ripple reduction and phase current control. In order to remove the effect by coupling relationship between control loops, an extra repetitive control branch is added in order to further optimize the performance of battery current control. Meanwhile, based on a unified model for motoring and regenerating modes, the proposed control scheme can achieve seamless transition between the two modes, which helps to restrain the overcurrent and improve the system reliability. Experimental results are presented to validate the feasibility and performance of the proposed control method.

The rest of this paper is organized as follows. In Section II, IMPC is briefly introduced. Based on that, a unified model covering the SRM and the converter is developed. Then, the two operation modes are discussed and a control method incorporating repetitive controller is proposed in Section III. Its steady-state performance, especially ripple control, is analyzed as well. Subsequently, the seamless transition function is briefly discussed. A set of simulation and comparative experimental results including waveforms for steady state and transient process are provided in Section V. Finally, conclusions are drawn in Section VI.

II. IMPC as SRM Drive

A multiphase converter is indispensable for transferring energy between the battery pack and SRM. Among various topologies, the asymmetric half-bridge (ASHB) topology in Fig. 1(b) is commonly used because of its simplicity. The waveform of phase current injected to SRM is shown in Fig. 2(a), and the relationship between the magnetic energy stored in one phase of SRM and current is illustrated in Fig. 2(b). However, the sudden change of power during current commutation periods cannot be handled by the ASHB. This leads to drastic change in the output power of the battery pack, causing periodic high peak current and high *di/dt* for the battery. In order to reduce this current ripple, Cai and Yi

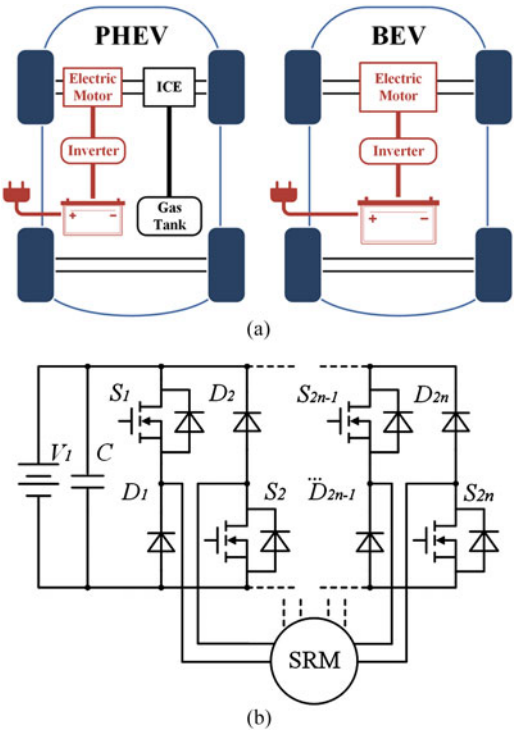

Fig. 1. Application of SRM: (a) configuration of PHEV&BEV, (b) the SRM drive system.

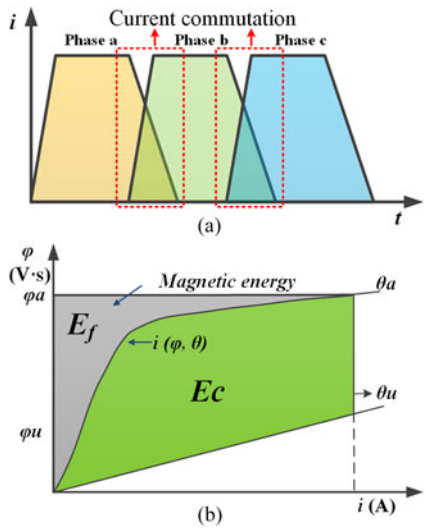

Fig. 2. SRM current commutation: (a) the phase current, (b) magnetic energy stored in SRM versus current.

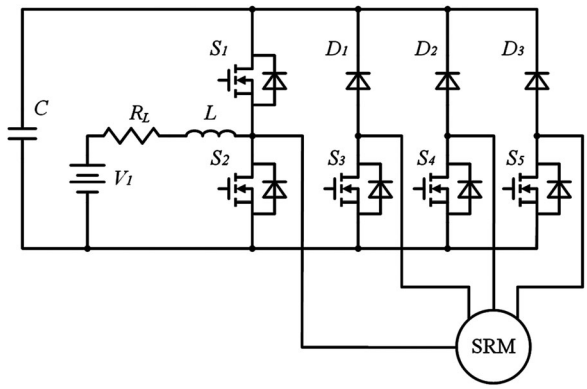

Fig. 3. IMPC as SRM drive.

Compared to asymmetrical H-bridge converter, the presented IMPC has several advantages. These advantages include

1) The capacitor is separated from the dc source. Hence, the dc source voltage will not be affected by the capacitor.
2) Both the average voltage and the ripple voltage of the capacitor can be large which allows for reduction of the capacitance requirement as much as possible.
3) The current through the dc source is filtered by an inductor, thus no electrolytic capacitor in parallel with the input dc source is necessary. Moreover, the requirement for the dc source voltage is loosen and can be lower than what the SRM needs (i.e., it does not act as dc link).
4) The dc-link voltage is flexible. By increasing the dc-link voltage, the time for de-energizing phases decreases so that conduction angle could be increased and larger average torque could be obtained. The speed range is widened which is especially appealing for high-speed applications.
5) Only five switches, three diodes, one inductor, and one small capacitor are needed in the IMPC in a three-phase SRM drive which means lower cost and higher power density in the motor drive. If the SRM contains n phases, n + 1 legs are necessary so that n + 2 switches and n diodes are needed in total.
6) Only n + 1 wires are required to drive an n phase SRM, which means less bulky wire harness.

In addition, similar to the ASHB, the IMPC can handle bidirectional power transfer between the SRM and the dc source. This is usually a battery pack or fuel cell in vehicular applications.

Even though the current ripple and capacitance reduction brought by IMPC have been verified in [34], it mainly focuses on the motoring mode of operation. The generating mode has not been discussed using IMPC. In addition, a simple control method is employed to control the converter, which limits its performance. Because dc source current, output current as well as dc the capacitor voltage have to be controlled, a multiloop control method is necessary. Unfortunately, the coupling relationship between different loops has not been estimated yet. This relationship will generate disturbance for all of the control loops and worsen its ripple reduction capability. Therefore, an advanced control method applicable to both motoring and generating modes is desirable to improve the system performance

III. Proposed Generalized Control Method Based on Repetitive Control

When employing the IMPC topology instead of the ASHB in transferring power from the battery to the SRM, there are several control objectives for IMPC. The battery current and the phase current for SRM should be controlled at the same time. Also, the capacitor voltage has to be limited within a certain range according to the requirement of the SRM and the capacitor voltage rating. Under this circumstance, the control method becomes more complicated. Furthermore, [34] also indicates that large voltage ripple on dc capacitor cannot be ignored if the battery current is controlled at a constant value because the ripple power required by the SRM should be compensated by the dc capacitor. This voltage ripple can also complicate the controller design difficult. In order to properly design the controller, modeling and analysis of the drive and SRM are needed.

A. Modeling

There are two parts to be modeled, one is the proposed IMPC and the other one is the SRM. First, the models of the SRM and the IMPC are analyzed separately. The stator pole number of the SRM is denoted by n. The current through each phase is i_k, $k \in [1, n]$ and the current through the inductor is i_L. The bridge connected to the dc source is multiplexed, so there is only a single stage. It is desirable to establish a model of the entire system including both the IMPC and the motor windings. For the sake of simplicity, the mutual inductances between different phases are ignored, and speed of the motor is assumed to be constant considering that the time constant of the electrical circuit is much smaller than that of the mechanical system. Based on the average model of the converter with SRM's phase currents taken into account, (1) can be derived

$$\begin{cases} L\dfrac{di_L}{dt} = v_{\text{in}} - (1-d)\, v_C - R_L i_L \\ C\dfrac{dv_C}{dt} = (1-d)\left(i_L - \displaystyle\sum_{k=1}^{n} i_k\right) + \displaystyle\sum_{k=1}^{n} (1-d_k)\, i_k \end{cases} \tag{1}$$

where d is the duty cycle of switch S_2; d_1–d_k are the duty cycles of switches connected to phases 1 through k, respectively; i_L is the inductor current, i_1–i_k are phase currents of phases 1 through k, respectively; R_L is the resistance of the inductor; v_C is the voltage of the capacitor. It is assumed that the current in each phase is continuous when the phase is energized. It is assumed that the current through the SRM phases is I_{d1} (equals $\sum_{k=1}^{n} i_k$) and I_{d2} (equals $\sum_{k=1}^{n} (1-d_k) i_k$), the simplified model of IMPC is shown in Fig. 4.

Similarly, SRM can be modeled using electromagnetic equations. Considering that the flux linkage of a phase is related to both the position of the rotor and the current flowing through the phase, the equation for each phase of the SRM is expressed as follows:

$$\begin{aligned} v_k &= R_k i_k + \frac{d\varphi_k}{dt} = R_k i_k + \frac{\partial \varphi_k}{\partial i_k}\frac{di_k}{dt} + \frac{\partial \varphi_k}{\partial \theta_k}\frac{d\theta_k}{dt} \\ &= R_k i_k + L_k(\theta, i)\frac{di_k}{} + \frac{\partial L_k(\theta, i)}{}\omega i_k. \end{aligned} \tag{2}$$

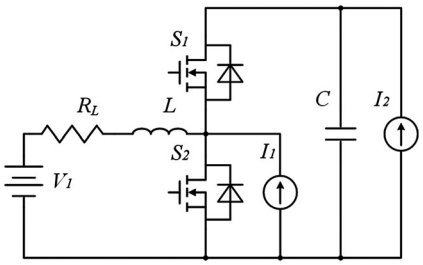

Fig. 4. Simplified model of the SRM drive system based on IMPC.

Also, the phase excitation voltage of the converter can be expressed as follows:

$$v_k = (1-d)\, v_c - (1-d_k)\, v_c = (d_k - d)\, v_c. \tag{3}$$

The electromechanical equations for SRM can be written as (4) using a simplified model introduced in [35]

$$\begin{cases} \dfrac{d\varphi}{dt} = v - Ri \\ \dfrac{d\omega}{dt} = \dfrac{1}{J}\left(T_e - T_L\right) \\ \dfrac{d\theta}{dt} = \omega \end{cases} \tag{4}$$

where φ is the flux, ω is the mechanical speed, T_e is the electromagnetic torque, T_L is the load torque, and J is the rotational inertia. The calculation of the parameters in generating mode and motoring mode are analyzed in sequence.

1) Magnetic Flux Linkage φ: The expression for φ is shown below. Since L is related to θ and i, the derivative of φ is expressed in terms of θ and L

$$\varphi = L(\theta, i)\, i \Rightarrow \frac{d\varphi}{dt} = i\omega\frac{dL}{d\theta} + \left(L + i\frac{dL}{di}\right)\frac{di}{dt}. \tag{5}$$

Considering that L is a periodic function of rotor position, θ can be expressed in form of Fourier series as shown in (6). For the sake of simplicity, only the first three orders are considered, as shown in (7)

$$L(\theta, i) = \sum_{n=0}^{\infty} L_n(i)\cos\left(nN_r\theta + \varphi_n\right) \tag{6}$$

$$\begin{aligned} L(\theta, i) = {} & AL_0(i) + AL_1(i)\cos\left(N_r\theta + \varphi_1\right) \\ & + AL_2(i)\cos\left(2N_r\theta + \varphi_2\right) \end{aligned} \tag{7}$$

where, the coefficient $AL_0(i)$, $AL_1(i)$, $AL_2(i)$ are expressed using the inductance at unaligned position (L_u), that at aligned position (L_a) and the inductance at the midway from the aligned position to the unaligned position (L_m)

$$\begin{cases} AL_0 = \dfrac{1}{2}\left(\dfrac{1}{2}\left(L_a + L_u\right) + L_m\right) \\ AL_1 = \dfrac{1}{2}\left(L_a - L_u\right) \\ AL_2 = \dfrac{1}{2}\left(\dfrac{1}{2}\left(L_a + L_u\right) - L_m\right). \end{cases} \tag{8}$$

Since saturation effect is negligible at unaligned position, L_u can be assumed constant. However, L_a and L_m are highly affected by phase currents because of the magnetic saturation. They can be approximated using polynomial functions given by

$$\begin{cases} L_a(i) = \sum_{n=0}^{k} a_n i^n \\ L_m(i) = \sum_{n=0}^{k} b_n i^n. \end{cases} \tag{9}$$

The inductance at unaligned position and aligned position stay the same for motoring mode and generating mode. If hysteresis effect is ignored, the midway inductance for the two modes should be the same as well. Otherwise, the midway inductance can be replaced with another coefficient: $L_{m\_m}(i) = \sum_{n=0}^{k} b_{n1} i^n$. Based on (5)–(9), (10) is obtained

$$\begin{cases} L + i\dfrac{dL}{di} = \dfrac{1}{2}\left(\dfrac{1}{2}\left(BL_a - BL_u\right) + BL_m\right) \\ \qquad\qquad + \dfrac{1}{2}\left(BL_a - BL_u\right)\cos\left(N_r\theta\right) \\ \qquad\qquad + \dfrac{1}{2}\left(\dfrac{1}{2}\left(BL_a + BL_u\right) - BL_m\right)\cos\left(2N_r\theta\right) \\ \dfrac{dL}{d\theta} = \dfrac{N_r}{2}\left(\left(BL_a - BL_u\right)\sin\left(N_r\theta\right)\right. \\ \qquad\qquad \left. + \left(BL_a - BL_u - 2BL_m\right)\sin\left(2N_r\theta\right)\right) \end{cases} \tag{10}$$

where the coefficients are calculated as

$$\begin{cases} BL_a(i) = \sum_{n=0}^{k} (n+1)\, a_n i^n \\ BL_m(i) = \sum_{n=0}^{k} (n+1)\, b_n i^n \end{cases},$$

and the coefficient BL_u is fixed as L_u. The derivative of φ in (5) can be rewritten as

$$\begin{aligned} \frac{d\varphi}{dt} = {} & \frac{N_r}{2} i\omega\left(\left(L_a - L_u\right)\sin\left(N_r\theta\right)\right. \\ & \left. + \left(L_a - L_u - 2L_m\right)\sin\left(2N_r\theta\right)\right) \\ & + \frac{1}{2}\left(\left(\frac{1}{2}\left(BL_a - BL_u\right) + BL_m\right)\right. \\ & + \left(BL_a - BL_u\right)\cos\left(N_r\theta\right) \\ & \left. + \left(\frac{1}{2}\left(BL_a + BL_u\right) - BL_m\right)\cos\left(2N_r\theta\right)\right)\frac{di}{dt}. \end{aligned} \tag{11}$$

2) Electromagnetic Torque T_e: From the coenergy relations, the electromagnetic torque can be developed as a closed form solution based on the phase current and the inductance at each position

$$\begin{aligned} T_e = {} & -\frac{N_r}{4} i^2\left(\left(CL_a - CL_u\right)\sin\left(N_r\theta\right)\right. \\ & \left. + \left(CL_a - CL_u - 2CL_m\right)\sin\left(2N_r\theta\right)\right) \end{aligned} \tag{12}$$

In (12), the coefficients are summarized as

$$\begin{cases} CL_a(i) = \sum_{n=0}^{k} \dfrac{2}{n+2} a_n i^n \\ CL_m(i) = \sum_{n=0}^{k} \dfrac{2}{n+2} b_n i^n \end{cases},$$

and the coefficient CL_u equals L_u. For motoring mode, the phase current exists in the range [0°, 180°] for θ. Under this condition, T_e is positive. For generating mode, phase current is applied in the range of [180°, 360°] for θ. Therefore, T_e becomes negative. No matter SRM operates in motoring mode or generating mode, (12) is valid. Moreover, all the coefficients (CL_u, CL_m, and CL_a) should be the same for motoring mode and generating mode, which means that the equivalent model does not change during mode transition and a generalized control solution is potential to cover various modes.

Combining (10)–(12), one can get the state-space equations of the SRM drive system, which is shown in (13) at the bottom the page.

Since the inductance of each phase depends on both the rotor position and the current, it is time variant and nonlinear. It is preferred to linearize it around a steady-state operation point. By linearization, the system performance can be analyzed, and then the corresponding controller design can be completed. However, since the magnetic saturation of the SRM will affect the operation point, it is necessary to verify the closed-loop stability using the large-signal model after inserting the controller.

Considering that the rate of variation in rotor speed is much smaller than that of voltage and current, speed can be assumed to be a constant (i.e., $\omega = d\theta/dt$is fixed). Rewriting (13), the equivalent model is shown in form of state-space equations as follows:

$$\begin{cases} x' = Ax + Bu \\ y = Cx \end{cases} \tag{14}$$

where, $x = [v_c, i_L, i_1, i_2, \ldots i_n]^T$, $u = [v_{in}, d, d_1, d_2, \ldots d_n]^T$, $y = [i_L, i_1, \ldots, i_n]^T$

$$A = \begin{bmatrix} 0 & \dfrac{1-D}{C} & \dfrac{D-D_1}{C} & \cdots & \dfrac{D-D_n}{C} \\ -\dfrac{1-D}{L} & -\dfrac{R_L}{L} & 0 & \cdots & 0 \\ \dfrac{2(D_1-D)}{M} & \dfrac{-2R_1 - N_r\omega N}{M} & 0 & \cdots & 0 \\ \cdots & \cdots & 0 & \cdots & 0 \\ \dfrac{2(D_n-D)}{M} & \dfrac{-2R_n - N_r\omega N}{M} & 0 & \cdots & 0 \end{bmatrix}$$

$$B = \begin{bmatrix} 0 & \dfrac{\sum_{k=1}^{n} I_k - I_L}{C} & -\dfrac{I_1}{C} & \cdots & -\dfrac{L_n}{C} \\ \dfrac{1}{L} & \dfrac{V_c}{L} & 0 & \cdots & 0 \\ 0 & \dfrac{-2V_c}{M} & \dfrac{2V_c}{M} & 0 & 0 \\ 0 & \dfrac{-2V_c}{M} & 0 & \dfrac{2V_c}{M} & 0 \\ 0 & \dfrac{-2V_c}{M} & 0 & 0 & \dfrac{2V_c}{M} \end{bmatrix},$$

$$C = \begin{bmatrix} 0 & 0 & 0 & \cdots & 0 \\ 0 & 1 & 0 & \cdots & 0 \\ 0 & 0 & 1 & \cdots & 0 \\ \cdots & \cdots & \cdots & \cdots & \cdots \\ 0 & 0 & 0 & \cdots & 1 \end{bmatrix}$$

$$\begin{cases} M = \left(\dfrac{1}{2}(BL_a - BL_u) + BL_m\right) + (BL_a - BL_u)\cos(N_r\theta) \\ \qquad + \left(\dfrac{1}{2}(BL_a + BL_u) - BL_m\right)\cos(2N_r\theta) \\ N = (L_a - L_u)\sin(N_r\theta) + (L_a - L_u - 2L_m)\sin(2N_r\theta) \end{cases}$$

where *D* represents the duty cycle of the lower switch in the common leg and D_1–D_n are the duty cycles for the lower switches in the other legs which correspond to each stator phase of the SRM.

$$\begin{cases} L\dfrac{di_L}{dt} = v_{\text{in}} - (1-d)v_c - R_L i_L \\ C\dfrac{dv_c}{dt} = (1-d)i_L + \sum_{k=1}^{n}(d-d_k)i_k \\ \dfrac{di_k}{dt} = \dfrac{2\left((d_k-d)v_c - R_k i_k - \dfrac{N_r}{2} i_k \omega\left((L_a - L_u)\sin(N_r\theta) + (L_a - L_u - 2L_m)\sin(2N_r\theta)\right)\right)}{\left(\dfrac{1}{2}(BL_a - BL_u) + BL_m\right) + (BL_a - BL_u)\cos(N_r\theta) + \left(\dfrac{1}{2}(BL_a + BL_u) - BL_m\right)\cos(2N_r\theta)}, k \in [1,n] \\ \dfrac{d\omega}{dt} = \dfrac{1}{J}\left(-\dfrac{N_r}{4} i^2\left((CL_a - CL_u)\sin(N_r\theta) + (CL_a - CL_u - 2CL_m)\sin(2N_r\theta)\right) - T_L\right) \\ \dfrac{d\theta}{dt} = \omega \end{cases} \tag{13}$$

Even though speed variation is slow, the coefficients in (14) are changing following θ. One can simplify the equations according to the specific operational condition of the SRM. For instance, during most of the time, there is only one motor phase working and the others are in idle mode. Hence, the number of the state-space equations in (17) can be limited at 3. Meanwhile, if one uses hysteresis control method to keep the SRM phase current constant, the effect caused by the dc bus voltage can be ignored. Then, the SRM phase current can be considered as disturbance for the inductor current control and the dc bus voltage control.

The phase inductance is assumed to be constant and the derivative of phase inductance with respect to position θ is also assumed to be constant. At certain position, these two parameters can be obtained with (7) and expressed as (16). Variables are perturbed as shown in

$$\begin{cases} i_L = I_L + \tilde{i}_L \\ v_C = V_C + \tilde{v}_C \\ i_k = I_k + \tilde{i}_k \end{cases} \tag{15}$$

$$\begin{cases} L_k(\theta, i) = L_k = AL_0(i) + AL_1(i)\cos(N_r\theta + \varphi_1) \\ \qquad\qquad +AL_2(i)\cos(2N_r\theta + \varphi_2) \\ \dfrac{\partial L_k(\theta, i)}{\partial\theta} = K = N_r AL_1(i)\sin(N_r\theta + \varphi_1) \\ \qquad\qquad +2N_r AL_2(i)\sin(2N_r\theta + \varphi_2). \end{cases} \tag{16}$$

For the SRM, only one phase is energized during most of the time. Hence, if only the current flowing through one phase is considered, the small signal model can be derived as shown in

$$\begin{cases} L\dfrac{d\tilde{i}_L}{dt} = -(1-D)\tilde{v}_C + V_c\tilde{d} - R_L\tilde{i}_L \\ C\dfrac{d\tilde{v}_C}{dt} = (1-D)\tilde{i}_L - I_L\tilde{d} + (D-D_k)\tilde{i}_k + I_k(\tilde{d} - \tilde{d}_k) \\ L_k\dfrac{d\tilde{i}_k}{dt} = V_c\left(\tilde{d}_k - \tilde{d}\right) + (D_k - D)\tilde{v}_C - R_k\tilde{i}_k - K\omega\tilde{i}_k, \end{cases}$$
$k \in [1, n]$. (17)

There are three output variables and two input variables in this model. However, the control loops for each of the three variables will have separate bandwidths. The phase current control loop should be designed to have the highest bandwidth while the dc capacitor voltage control loop has the lowest bandwidth. As a result, the model can be analyzed as separate single-input-single-output subsystems. Taking the Laplace transform of (17), the relationship between i_L, i_k and duty cycles *d, d_k* can be derived as shown in

$$i_L(s) = \frac{J(s)}{T(s)} \times d(s) \tag{18}$$

where

$$\begin{cases} J(s) = -\dfrac{CsV_c}{1-D} + I_k - I_L - \dfrac{(D-D_k)V_c}{L_k s + R_k + K\omega} \\ \qquad -\dfrac{(D-D_k)^2 V_c}{(L_k s + R_k + K\omega)(1-D)} \\ T(s) = -\dfrac{Cs(Ls + R_L) + (1-D)^2}{1-D} \\ \qquad -\dfrac{(D-D_K)^2(Ls + R_L)}{(L_k s + R_k + K\omega)(1-D)}. \end{cases} \tag{19}$$

B. Coupling Relationship

Since that the input current, the output current, and the dc capacitor voltage should be controlled, the overall system is multiple input and multiple output. The coupling relationship has to be addressed especially between the input current and output current. The experimental results in Section IV will indicate the effect caused by coupling relationship. According to the simplified model in Fig. 4, the state-space equations in (20) can be derived as

$$\begin{cases} L\dfrac{di_L}{dt} = v_{\text{in}} - i_L R_L - (1-d)v_c \\ C\dfrac{dv_c}{dt} = (1-d)(i_L + I_{d1}) + I_{d2}. \end{cases} \tag{20}$$

Subsequently, the transfer functions from the different disturbance sources, i.e., I_{d1} and I_{d2}, to the current ripple in the inductor are derived. The dependence of disturbance upon the system can be analyzed using the transfer functions

$$G_{d1}(s) = \frac{i_L(s)}{I_{d1}(s)} = -\frac{(1-D)^2}{LCs^2 + R_L Cs + (1-D)^2} \tag{21}$$

$$G_{d2}(s) = \frac{i_L(s)}{I_{d2}(s)} = -\frac{1-D}{LCs^2 + R_L Cs + (1-D)^2}. \tag{22}$$

The main frequency of the current ripple is determined as the phase excitation scheme. If all stator phases are excited using the same turn-on and turn-off angles and the same current magnitude, the main frequency can be obtained as

$$f_m = N \times n_{\text{phase}} \times n_{\text{pole,rotor}} \tag{23}$$

where, *N* is the mechanical speed of the shaft and is measured in revolutions per second. However, if the phases are excited differently, a lower frequency component will be significant

$$f_m = N \times n_{\text{pole,rotor}}. \tag{24}$$

The values of the circuit elements and the configuration of the SRM used in the experiments and the calculation of transfer functions are listed in Table I in Section IV.

Assuming that the SRM analyzed here operates in the speed range of 1000 to 2000 r/min. The steady-state duty cycle of the upper switch is set at 0.5, which means that the voltage of the capacitor is controlled at twice the voltage of the battery theoretically. Then, the parameters in Table I can be inserted into the transfer functions (21) and (22) to obtain their Bode

TABLE I
PARAMETERS OF THE MOTOR DRIVES IN EXPERIMENTS

ASHB	
Parameter	Value
Input voltage	280 V
Switches	STGIPS30C60∗2
Dc bus capacitor	660 μf
IMPC	
Parameter	Value
Input voltage	110.0-128.0 V
Dc bus voltage	280 V
Switches	STGIPS30C60
Switching frequency	20 KHz
Inductor	540 μH, 24 mΩ
Dc bus voltage	250–350 V
Dc bus capacitor	220 μF

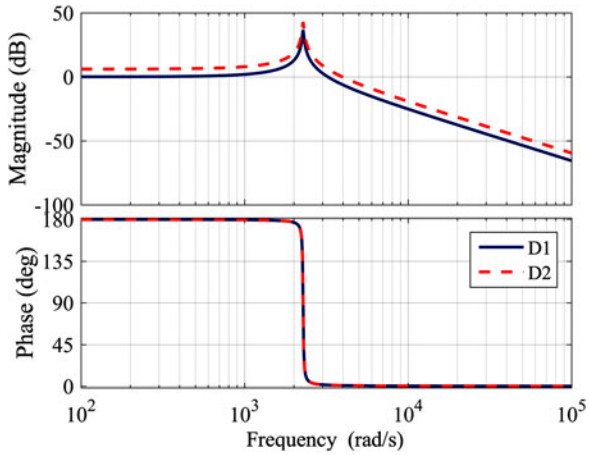

Fig. 5. Bode plots for the transfer functions from the two sources of disturbance to the battery current.

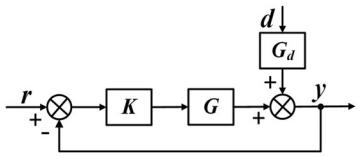

Fig. 6. General one degree-of-freedom feedback control system model for input current control.

plots. The Bode plots of the above transfer functions are shown in Fig. 5.

The above transfer functions and the corresponding Bode plots show a very high gain from the disturbance to the input current at the frequency range corresponding to the assumed speed range of the SRM. Specifically, the gain is about 3.3 dB for transfer function G_{d1} and 9.3 dB for transfer function G_{d2} at 200 Hz, which is the main frequency component caused by the large disturbing currents when the motor is running at a speed of 1000 r/min. Ignoring the measurement errors, the current control loop can be modeled using the general one degree-of-freedom feedback control system model shown in Fig. 6, where *K(s)* is the controller, *G(s)* is the plant, and $G_d(s)$ is the transfer function from disturbance to the output of the system that can

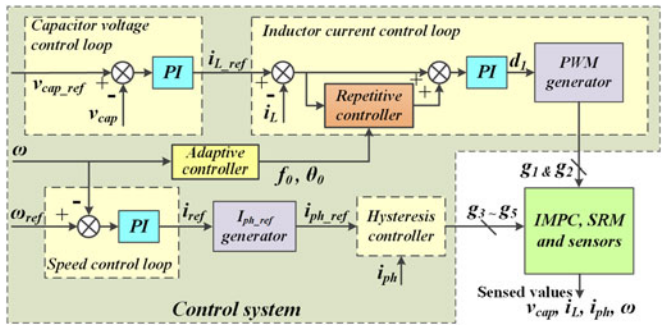

Fig. 7. Power flow control of the dc port for IMPC.

be G_{d1} or G_{d2} in the previous equations (21) and (22). The error sensitivity function to disturbance can be expressed as

$$S_r = (I + KG)^{-1} G_d. \tag{25}$$

From the state-space equations (20), the transfer function for the plant G can be derived as

$$G(s) = \frac{i_L(s)}{D(s)} = -\frac{(1-D)I + V_c C s}{LCs^2 + R_L C s + (1-D)}. \tag{26}$$

In (25), it is shown that G_d can be very large at a frequency range of disturbance d. Due to its limited gain at higher frequency, using a simple PI controller as *K(s)* in Fig. 6 cannot ensure a small value of S_r to suppress the output error at that frequency range. This reveals that the input current from the dc source is impacted by the current fluctuation incurred by the SRM, and that a simple PI controller will not be able to successfully eliminate this effect. A properly designed plug-in repetitive controller will be designed and inserted into *K(s)* to provide enough gain at the frequencies where the input current is disturbed to negate this impact.

C. Generalized Multiloop Control Method

The proposed control method has been shown in Fig. 7. There are two control branches, one is IMPC control including dc capacitor voltage and battery current, and the second one is the SRM control with speed/torque and phase current. In the IMPC control branch, the average dc capacitor voltage is detected and regulated at a constant value. The output of this control loop is the battery current reference. With the detected battery current, the duty cycle of the first leg is regulated to make the battery current track the reference. In the inner loop, repetitive controller is inserted in series with PI controller to reduce the low-frequency ripple which cannot be restrained using the PI controller alone. On the other hand, in the SRM control branch, the speed or torque is expected to be regulated. The output of this control loop is the reference for phase currents. Subsequently, the phase current is regulated using a hysteresis controller and the dynamic performance is guaranteed. In Fig. 3, g_1 and g_2 are the PWM signals for S_1 and S_2, respectively. Meanwhile, g_3, g_4, and g_5 are the signals for S_3, S_4, and S_5.

There is a phase current generation unit I_{ph_ref} in Fig. 7. This unit is to transfer the peak current command i_{ref} to phase current in each winding. The calculation method is given by (27). θ is the electrical rotor angel which increases from 0° to

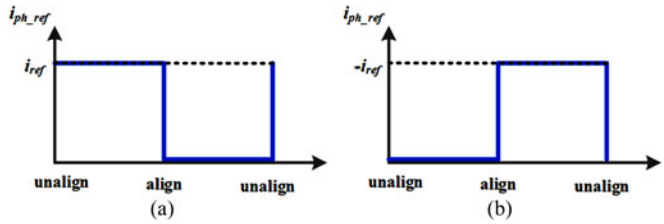

Fig. 8. Phase current reference: (a) motoring mode, (b) generating mode.

360°. From (27), when the current command is positive, the phase current command equals $i_{\rm ref}$ when the rotor goes from unaligned position to aligned position. When the rotor passes the aligned position, the phase current reference drops to 0, as Fig. 8(a) shows. Under this condition, the motor works in motoring mode. Otherwise, when the current command is negative, the phase current keeps 0 before the rotor goes through the aligned position. After that, the current becomes the absolute value of the current reference as shown in Fig. 8(b). This represents generating mode of operation

$$i_{ph\_\rm ref} = \frac{abs\left(i_{\rm ref}\right)}{2} + \frac{\rm sgn\left(180^\circ - \theta\right)}{2} i_{\rm ref} \tag{27}$$

where

$$sgn\left(x\right) = \begin{cases} 1, & x > 0 \\ -1, & x < 0 \end{cases}$$

.

From the proposed control method, it can also be seen that the bandwidth of dc capacitor voltage control loop is less than battery current control bandwidth because the battery current control is considered as an inner loop. This would make the dc capacitor to provide the low-frequency power ripple and restrain the current ripple of the battery. Another advantage is that the energy difference during the dynamic response time would also be compensated by the dc capacitor instead of battery. It could remove the overcharging or discharging condition and expand the battery lifetime.

D. Repetitive Controller Design

Section III.C has revealed the coupling between the phase current and the battery current. It is difficult to reduce the current ripple by using the conventional PI controller in the battery current control loop. Therefore, a repetitive controller is inserted into the battery current control loop. The frequency response of the repetitive controller used in this system is shown in Fig. 9. It can be seen that in the fundamental frequency and its harmonics, though the low-pass filter suppresses the gain of the repetitive controller, it still has very high gains. Thus, a good steady-state performance of the proposed control method can be expected. However, because of the fact that the frequency of the phase current would vary following the rotor speed, another adaptive controller is embedded into the control method as in Fig. 8. This adaptive controller outputs the fundamental frequency of the repetitive controller and compensates for the phase shift caused by detection delay.

In the repetitive controller, a low-pass filter is needed to ensure the stability of the control system [36]. Due to the fact that the

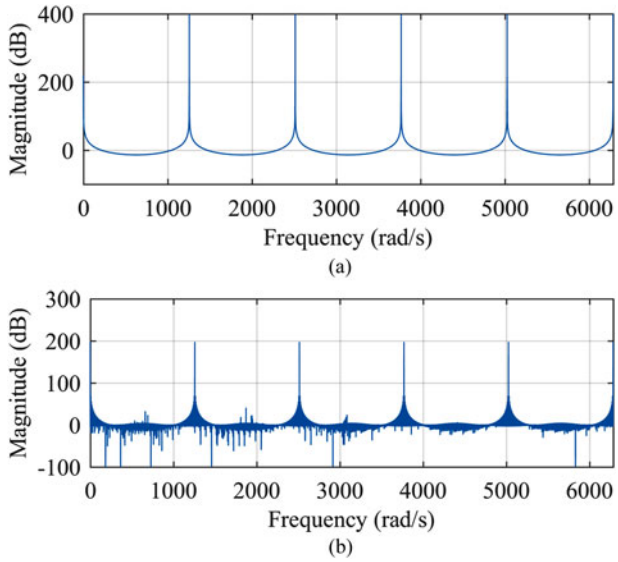

Fig. 9. Frequency responses of repetitive controller (a) without any filters, (b) with moving average filter.

filtered results are not needed instantly and will be fed into the control loop in the next period, it is possible to implement zero-phase low-pass filters, which are noncausal. A simple finite impulse response moving average low-pass filter (28) is used in this paper because it is easy to design and implement in digital microcontrollers

$$y_n = \frac{1}{2n+1} \sum_{i=n-q}^{n+q} x_i. \tag{28}$$

Inserting the low-pass filter into the repetitive controller, the new transfer function can be expressed as (29), where *q(s)* is the transfer function of the low-pass filter

$$K_r = \frac{1}{1 - q(s)e^{-s/f}}. \tag{29}$$

There are also other possible choices for low-pass filters which can bring advantages to the performance of the repetitive controller. More discussions on the design of the low-pass filter can be found in the literatures, such as [37] and [38].

E. Seamless Transition

From the electromagnetic torque described in (12), it can be seen that the theoretical model is able to cover both motoring mode and generating mode of operation. By exciting the phases during $N_r\theta \in [0, 180^\circ]$, the torque would be positive which means that SRM works at motoring mode. Opposite, when the phase is excited at the range $N_r\theta \in [180^\circ, 360^\circ]$, the electromagnetic torque would be negative.

The speed/torque control loop in Fig. 6 shows that when the speed or torque is too high, the current reference would decrease or even become negative. The corresponding electromagnetic torque would decrease from positive to negative smoothly. During this transient period, SRM switches from the motoring mode to generating mode without overshoot. At the same time, the extra energy would be injected into the dc capacitor and lead to capacitor voltage increase. In order to keep the capacitor average

voltage constant, the inductor current would also be regulated to a negative value by the IMPC branch in the control scheme. Thus, eventually the energy is transferred into the battery. This function benefits EVs, because the energy is desirable to be absorbed by the battery instead of wasted when braking or decreasing speed. With this advantage, the efficiency of the overall system can be improved. Conversely, in order to speed up the SRM, the capacitor voltage would decrease as a result of more electromagnetic torque being generated. Consequently, the battery current increases to boost the dc capacitor average voltage.

IV. Simulation and Experimental Results

The feasibility and the control performance with conventional control methods using IMPC have been verified with simulation and experiments in [34]. In this paper, comparison of steady-state and dynamic performance between these two topologies at generating mode of operation is developed with emphasis on the dc port and the dc bus capacitor voltage. The detailed parameters of the IMPC and ASHB are all listed in Table I. The switching frequency is selected to be 20 kHz in consideration of the power rating of the SRM and the dc bus voltage. After that, two test-beds based on the IMPC and the ASHB are built and used to drive the same two-phase SRM experimentally. The corresponding experimental results will be displayed to compare their performance.

A. Simulation Results

Simulation model based on IMPC with three-phase symmetrical SRM is built in MATLAB/Simulink in order to verify the feasibility of IMPC at generating mode since Fig. 10 shows the steady-state waveforms at generating mode including the flux [see Fig. 10(a)], the torque [see Fig. 10(b)], the battery current [see Fig. 10(c)], and the capacitor voltage [see Fig. 10(d)]. Even though the torque ripple [see Fig. 10(b)] is large which needs large power ripple through the converter, the battery current is controlled at a constant value (2 A) with small ripple (0.18 A peak-to-peak) in Fig. 10(c). The power ripple is compensated by the dc capacitor which leads to 40 V peak-to-peak voltage ripple as shown in Fig. 10(d).

Fig. 11 indicates the dynamic performance under test. At first, the speed is controlled at 1000 r/min as shown in Fig. 11(a). When t = 0.1 s, the load torque changes from –4.5 N·m to –6 N·m. It can be seen that the speed of the SRM goes up after this step change in torque. However, 100 ms later, it goes back to 1000 r/min again. Fig. 11(b) and (c) shows the three-phase current waveforms during this dynamic process. As shown in Fig. 11(d), at the beginning of the transient process, the dc capacitor is charged by SRM, and then the voltage is regulated back to 280 V. Both the phase current and battery current increase smoothly with less than 11% overshoot and 250 ms dynamic response time.

B. Experimental Results

Two prototypes are built based on the conventional ASHB topology and the proposed IMPC in order to compare their performances. Here, ten 12-V automotive lead-acid batteries are connected in series as the dc source to drive an SRM. The SRM used employs a two-phase two-stack structure with each stack having eight stator poles and eight rotor poles. The coils on the stator of each stack are connected in series to form one phase, and the two stacks are shifted with respect to each other to allow reliable startup and smooth operation. The cross section of the SRM used in the experiments is shown in Fig. 12(a). A detailed analysis of the motor structure can be found in [34]. Each phase winding has one end connected to the common leg consisted of two switches and the other end connected to legs consisted of one diode and one switch. A dc alternator is coupled to the SRM as load or prime mover. The dc alternator is driven by a dc power supply in parallel with dc load. The converters are built with an intelligent molded module STGIPS30C60 from STMicroelectronics. The maximum IGBT collector emitter voltage used in the power converter is 600 V and the continuous collector current is 30 A. The switching frequency is still 20 kHz. The prototype is shown in Fig. 12. Major parameters are listed in Table I. Three cases are compared with experimental waveforms: ASHB with PI controllers, IMPC with PI controllers, and IMPC with proposed control method. All these three

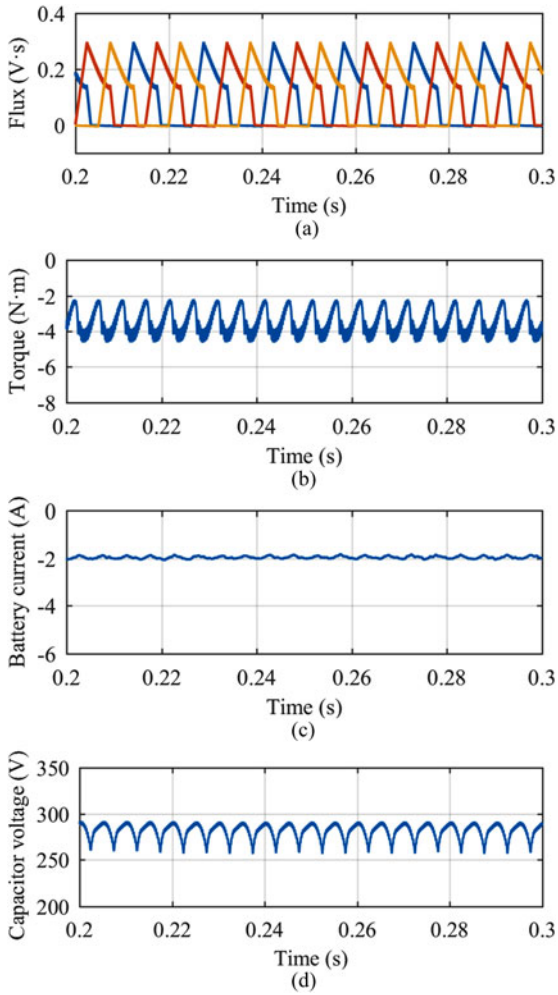

Fig. 10. Steady-state waveform in simulation: (a) flux, (b) torque, (c) battery current, (d) dc capacitor voltage.

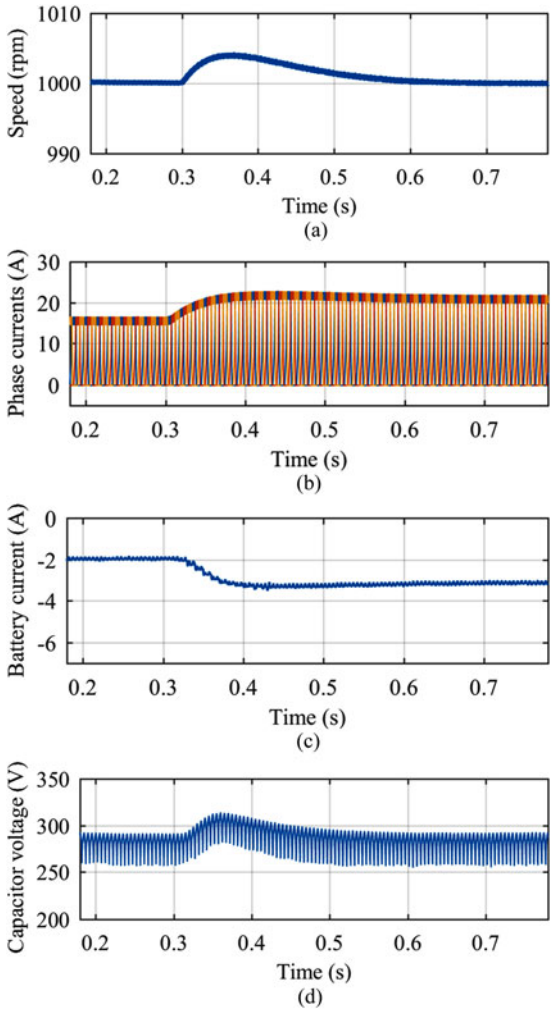

Fig. 11. Dynamic waveforms (in simulation): (a) speed, (b) phase current, (c) battery current, (d) dc capacitor voltage.

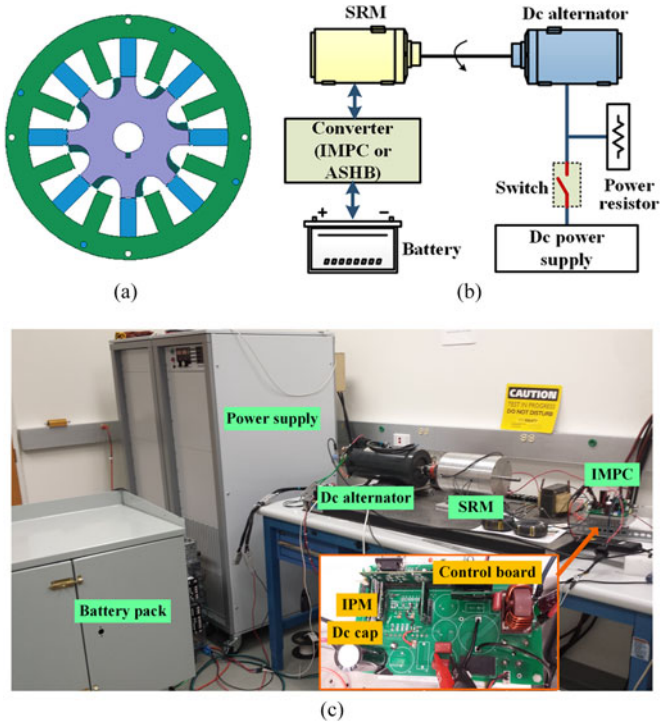

Fig. 12. Prototype of the SRM drive system: (a) cross section of the motor, (b) configuration of prototype, (c) picture of the setup.

control methods are implemented digitally using Texas Instruments' microcontroller unit TMS320F28335.

The average dc capacitor voltage is controlled at 280 V. Large voltage ripple on the dc capacitor can be observed because the capacitor is supposed to compensate the energy difference between the motor and the batteries during current commutation periods. However, it is also worth pointing out that the capacitance cannot be too small, because enough capacitor is needed to provide energy shortfall during startup and to keep the dc bus voltage in a reasonable range. Here, the capacitor is selected at 220 μF. This is to keep the voltage ripple less than 70 V to ensure that the lowest possible voltage is high enough so as not to impact the performance of the SRM drive, and to limit the voltage stress of capacitor and switches. As stated before, the proposed control method can be used in motoring and generating modes. Therefore, both modes are tested and steady-state waveforms are presented to verify its feasibility.

1) Motoring Mode: For the motoring mode of operation, the switch in Fig. 12(b) is OFF and the output of dc alternator is connected to resistor load alone. At this time, SRM is driven by the battery through the converter (ASHB or IMPC), hence, the energy is transferred from the battery to SRM. SRM converts the electric energy to mechanical energy with positive torque. DC alternator converts mechanical energy to electric energy and dissipates it with the resistor load.

Using the conventional ASHB as the drive, waveforms of the two motor phase current and input current are shown in Fig. 13(a). The two phases of the stator are driven alternatively according to the rotor position. For this converter, three 220-μF electrolytic capacitors are connected in parallel in the dc bus and at the input source. Even though large capacitors are used, the input current from the battery is still pulsatory and the peak-to-peak current is 13.8 A. Furthermore, the current becomes negative when the dc bus capacitor does not absorb enough energy during the de-energizing period of a stator phase. The proposed IMPC with conventional control method is tested under motoring mode of operation and the corresponding waveforms are shown in Fig. 13(b). The output current waveform is almost the same. However, the important difference is observed at the input port. The input current and the dc bus voltage are shown in Fig. 13(b)(CH2) and (b)(CH1), respectively. The frequency distributions of the input currents are shown in Fig. 13(c), which clearly shows 85% reduction of fundamental frequency component and more than 66% ripple reduction for other frequencies. There is a low-frequency voltage ripple on dc bus, however, the ripple of the input current is reduced significantly. The waveforms reveal that the peak-to-peak current is less than 2.8 A which is only 20% of the input current when ASHB converter is used.

Fig. 14(a) shows the steady-state waveform with reduced capacitors from 660 to 220 μF. Comparing such waveform with Fig. 13(b), it can be seen that the input current is almost the same, but the voltage ripple at the dc capacitor is enlarged which can

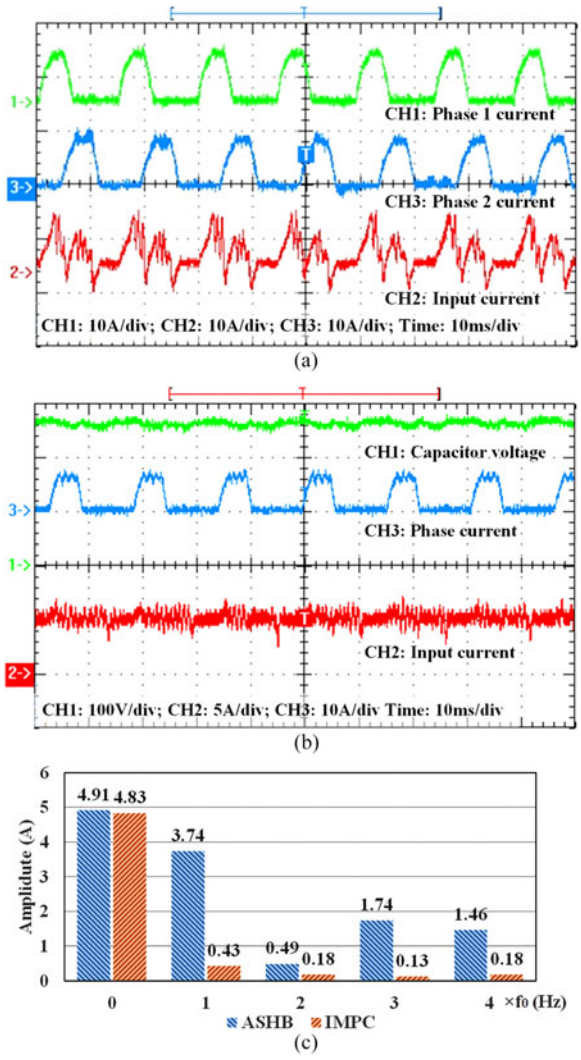

Fig. 13. Experimental results: (a) ASHB, (b) IMPC, (c) frequency distribution.

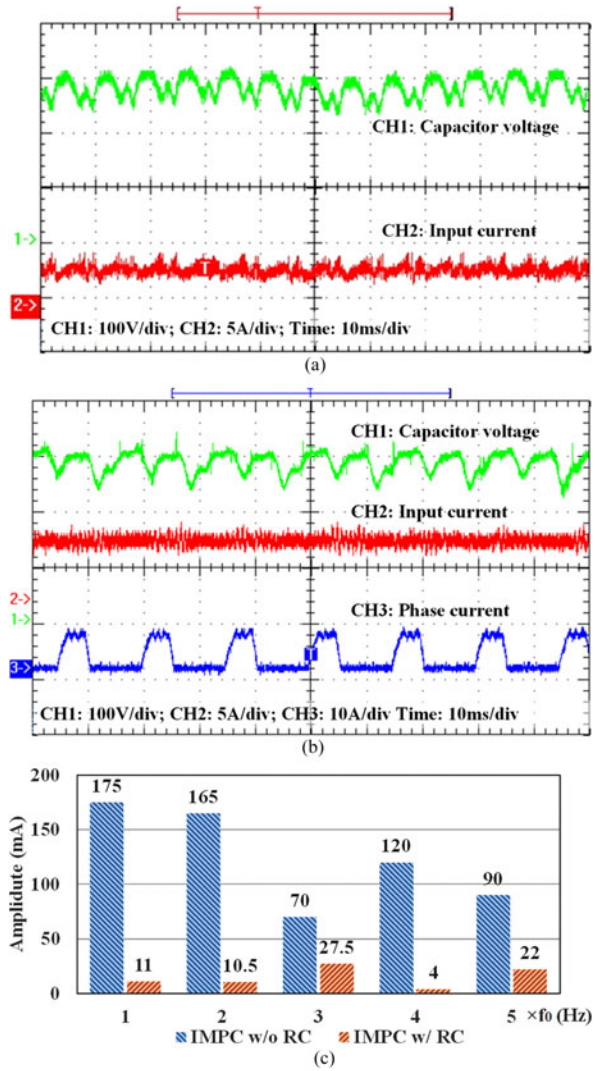

Fig. 14. Experimental results with 220 μF dc capacitor: (a) IMPC with conventional control, (b) IMPC with proposed control, (c) frequency distribution.

be estimated with theoretical analysis. After that, the proposed control method in Section III is implemented at the same test bed. The corresponding waveforms are shown in Fig. 14(b). It can be found that the current spike has been removed and the peak-peak value is 0.8 A (5.7% of the input current when compared to ASHB). The detailed frequency distribution is listed in Fig. 14(c) which reveals the significant current ripple reduction by using the presented control method.

The waveforms in Figs. 13 and 14 suggest that the proposed topology can act as the drive for SRM instead of the conventional ASHB topology and the control method presented in Section IV is suitable for the proposed topology.

2) Generating Mode: The generating mode of operation of the SRM is tested with the dc alternator driven by dc power supply (Switch in Fig. 12(a) is ON). When the alternator is connected to dc power supply and resistor load, it provides positive mechanical torque. At this time, SRM acts as load and it absorbs energy from the alternator. Meanwhile, IMPC is used to transfer the energy from SRM to the battery pack.

Fig. 15(a) shows the current through the battery when using the IMPC structure without proposed control method. The low-frequency ripple is too large to be ignored. Even though the average current is 3.99 A, the peak-to-peak value is 8.20 A. On the contrary, if using IMPC as well as the proposed control method, the battery current would be constant (3.84 A) with only a small ripple which is displayed in Fig. 15(b). The peak-to-peak ripple is limited in only 0.86 A. Moreover, from the frequency distribution in Fig. 15(c), the 200-Hz ripple is 0.24 A which is only 6% of that without proposed control method (4.05 A). In addition, all the other low-frequency ripples are decreased by at least 50%.

3) Seamless Transition: Fig. 16(a) shows the comparative results with/out repetitive controller. Without repetitive controller, the battery current contains 3.6 A peak-to-peak current ripple. After inserting repetitive controller, the peak-to-peak current ripple is decreased to 0.9 A. But the capacitor voltage ripple (peak-to-peak) is increased from 46.2 to 68.8 V because more power ripple is compensated by the capacitor instead of the battery. The dynamic performance of the presented control method is also tested with seamless transition capability. The experimental waveform is shown in Fig. 16(b). At the beginning, switch in Fig. 12(a) is OFF and SRM works in motoring mode.

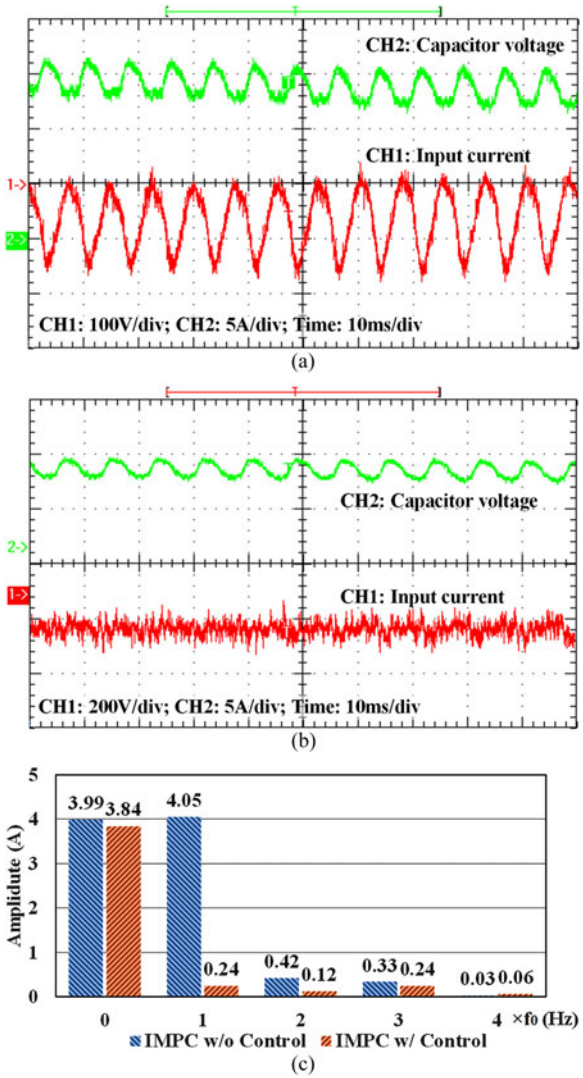

Fig. 15. Current through battery in experiments: (a) IMPC topology without proposed control method, (b) IMPC topology with proposed control method, (c) frequency distribution.

When switch is turned ON and the power supply is connected to dc alternator, SRM drive switches from motoring mode to generating mode of operation automatically. It can be seen that the dynamic time is 2.1 s and there is no overshoot of battery current during the dynamic process. In addition, there is 9% overshoot in dc capacitor voltage which does not exceed capacitor voltage rating.

In short, the above simulation and experimental results reveal that the proposed control method can keep the battery current ripple less than 6% of the average current and achieve seamless transition with no overshoot in battery current and 9% overshoot in dc capacitor voltage. This demonstrates the feasibility and superiority of the proposed control method.

V. Conclusion

A unified model covering motoring mode and generating mode for SRM drives is developed and a generalized control method with seamless transition ability based on the system model is presented in this paper. Power ripple resulted from

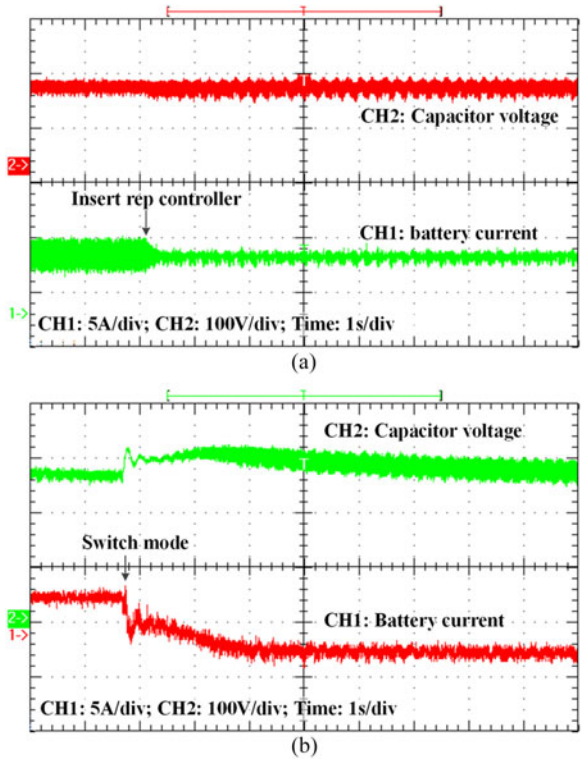

Fig. 16. Dynamic waveform in experiment: (a) inserting repetitive controller, (b) from motor mode to generation mode.

current commutation of SRM leads to large current ripple for battery which shortens the lifetime of the battery and decreases system efficiency. In order to overcome this disadvantage and harvest kinetic energy for EV applications, IMPC is chosen as the SRM drive topology and a corresponding control method that can significantly restrain the low-frequency ripple current of the battery is proposed. Seamless transition between generating mode and motoring mode can also be achieved with the proposed control method by employing a current reference generator using the unified model. This can enhance the converter's reliability and efficiency. The validity and stability of the proposed control method with IMPC is verified using simulation and experimental results. Comparative results reveal that 94% of periodical transient power ripple can be eliminated and smooth seamless transition with no current overshoot has been achieved.

Acknowledgment

This work was done in the Renewable Energy and Vehicular Technology Laboratory, the University of Texas at Dallas, Richardson, TX, USA. The authors would like to thank the founding director Dr. Babak Fahimi for his support.

References

[1] P. N. Materu and R. Krishnan, "Steady-state analysis of the variable-speed switched-reluctance motor drive," *IEEE Trans. Ind. Electrons.*, vol. 36, no. 4, pp. 523–529, Nov. 1989.

[2] M. Abbasian, M. Moallem, and B. Fahimi, "Double-stator switched reluctance machines (DSSRM): Fundamentals and magnetic force analysis," *IEEE Trans. Energy Convers.*, vol. 25, no. 3, pp. 589–597, Sep. 2010.

[3] B. Fahimi, A. Emadi, and R. B. Sepe, "A switched reluctance machine-based starter/alternator for more electric cars," *IEEE Trans. Energy Convers.*, vol. 19, no. 1, pp. 116–124, Mar. 2004.
[4] K. M. Rahman, B. Fahimi, G. Suresh, A. V. Rajarathnam, and M. Ehsani, "Advantages of switched reluctance motor applications to EV and HEV: Design and control issues," *IEEE Trans. Ind. Appl.*, vol. 36, no. 1, pp. 111–121, Jan./Feb. 2000.
[5] Y. Jin, B. Bilgin, and A. Emadi, "An extended-speed low-ripple torque control of switched reluctance motor drives," *IEEE Trans. Power Electron.*, vol. 30, no. 3, pp. 1457–1470, Mar. 2015.
[6] I. Boldea, L. N. Tutelea, L. Parsa, and D. Dorrell, "Automotive electric propulsion systems with reduced or no permanent magnets: An overview," *IEEE Trans. Ind. Electron.*, vol. 61, no. 10, pp. 5696–5711, Oct. 2014.
[7] L. Long and P. Bauer, "Practical capacity fading model for Li-ion battery cells in electric vehicles," *IEEE Trans. Power Electron.*, vol. 28, no. 12, pp. 5910–5918, Dec. 2013.
[8] F. Savoye, P. Venet, M. Millet, and J. Groot, "Impact of periodic current pulses on Li-ion battery performance," *IEEE Trans. Ind. Electron.*, vol. 59, no. 9, pp. 3481–3488, Sep. 2012.
[9] A. Hoke, A. Brissette, K. Smith, A. Pratt, and D. Maksimovic, "Accounting for lithium-ion battery degradation in electric vehicle charging optimization," *IEEE J. Emerg. Sel. Topics Power Electron.*, vol. 2, no. 3, pp. 691–700, Sep. 2014.
[10] M. Swierczynski, D. I. Stroe, A. I. Stan, R. Teodorescu, and S. K. Kaer, "Lifetime estimation of the nanophosphate LiFePO4 battery chemistry used in fully electric vehicles," *IEEE Trans. Ind. Appl.*, vol. 51, no. 4, pp. 3453–3461, Jul./Aug. 2015.
[11] G. Linlin, R. Xinbo, X. Ming, and Y. Kai, "Means of eliminating electrolytic capacitor in AC/DC power supplies for LED lightings," *IEEE Trans. Power Electron.*, vol. 24, no. 5, pp. 1399–1408, May 2009.
[12] J. L. Stevens, J. S. Shaffer, and J. T. Vandenham, "The service life of large aluminum electrolytic capacitors: effects of construction and application," *IEEE Trans. Ind. Appl.*, vol. 38, no. 5, pp. 1441–1446, Sep. 2002.
[13] C. Rodriguez and G. Amaratunga, "Long-lifetime power inverter for photovoltaic AC modules," *IEEE Trans. Ind. Electron.*, vol. 55, no. 7, pp. 2593–2601, Jul. 2008.
[14] L. Changrong and L. Jih-Sheng, "Low frequency current ripple reduction technique with active control in a fuel cell power system with inverter load," *IEEE Trans. Power Electron.*, vol. 22, no. 4, pp. 1429–1436, Jul. 2007.
[15] J. I. Itoh and F. Hayashi, "Ripple current reduction of a fuel cell for a single-phase isolated converter using a DC active filter with a center tap," *IEEE Trans. Power Electron.*, vol. 25, no. 3, pp. 550–556, Mar. 2010.
[16] W. Rong-Jong and L. Chun-Yu, "Active low-frequency ripple control for clean-energy power-conditioning mechanism," *IEEE Trans. Ind. Electron.*, vol. 57, no. 11, pp. 3780–3792, Nov. 2010.
[17] C. Wen, L. Bangyin, D. Shanxu, and J. Ling, "An active low-frequency ripple control method based on the virtual capacitor concept for BIPV systems," *IEEE Trans. Power Electron.*, vol. 29, no. 4, pp. 1733–1745, Apr. 2014.
[18] W. Rong-Jong and L. Chun-Yu, "Development of active low-frequency current ripple control for clean-energy power conditioner," in *Proc. 5th IEEE Conf. Ind. Electron. Appl.*, 2010, pp. 695–700.
[19] S. Mei, P. Pan, L. Xi, S. Yao, and Y. Jian, "An active power-decoupling method for single-phase AC/DC converters," *IEEE Trans. Ind. Informat.*, vol. 10, no. 1, pp. 461–468, Feb. 2014.
[20] W. Cai, L. Jiang, B. Liu, S. Duan, and C. Zou, "A power decoupling method based on four-switch three-port DC/DC/AC converter in DC microgrid," *IEEE Trans. Ind. Appl.*, vol. 51, no. 1, pp. 336–343, Jan./Feb. 2015.
[21] P. T. Krein, R. S. Balog, and M. Mirjafari, "Minimum energy and capacitance requirements for single-phase inverters and rectifiers using a ripple port," *IEEE Trans. Power Electron.*, vol. 27, no. 11, pp. 4690–4698, Nov. 2012.
[22] X. Liu, Z. Q. Zhu, M. Hasegawa, A. Pride, R. Deohar, T. Maruyama *et al.*, "Dc-link capacitance requirement and noise and vibration reduction in 6/4 switched reluctance machine with sinusoidal bipolar excitation," in *Proc. IEEE Energy Convers. Congr. Expo.*, 2011, pp. 1596–1603.
[23] C. R. Neuhaus and R. W. De Doncker, "DC-link voltage control for switched reluctance drives with reduced DC-link capacitance," in *Proc. IEEE Energy Convers. Congr. Expo.*, 2010, pp. 4192–4198.
[24] C. R. Neuhaus, N. H. Fuengwarodsakul, and R. W. De Doncker, "Control scheme for switched reluctance drives with minimized DC-link capacitance," *IEEE Trans. Power Electron.*, vol. 23, no. 5, pp. 2557–2564, Oct. 2008.
[25] W. Suppharangsan and J. Wang, "Experimental validation of a new switching technique for DC-link capacitor minimization in switched reluctance machine drives," in *Proc. IEEE Int. Electr. Mach. Drives Conf.*, 2013, pp. 1031–1036.
[26] L. Guangjin, J. Ojeda, S. Hlioui, E. Hoang, M. Lecrivain, and M. Gabsi, "Modification in rotor pole geometry of mutually coupled switched reluctance machine for torque ripple mitigating," *IEEE Trans. Magn.*, vol. 48, no. 6, pp. 2025–2034, Jun. 2012.
[27] P. C. Desai, M. Krishnamurthy, N. Schofield, and A. Emadi, "Novel switched reluctance machine configuration with higher number of rotor poles than stator poles: Concept to implementation," *IEEE Trans. Ind. Electron.*, vol. 57, no. 2, pp. 649–659, Feb. 2010.
[28] R. Mikail, I. Husain, Y. Sozer, M. S. Islam, and T. Sebastian, "Torque-ripple minimization of switched reluctance machines through current profiling," *IEEE Trans. Ind. Appl.*, vol. 49, no. 3, pp. 1258–1267, May 2013.
[29] S. K. Sahoo, S. Dasgupta, S. K. Panda, and X. Jian-Xin, "A lyapunov function-based robust direct torque controller for a switched reluctance motor drive system," *IEEE Trans. Power Electron.*, vol. 27, no. 2, pp. 555–564, Feb. 2012.
[30] H. J. Brauer, M. D. Hennen, and R. W. De Doncker, "Control for polyphase switched reluctance machines to minimize torque ripple and decrease ohmic machine losses," *IEEE Trans. Power Electron.*, vol. 27, no. 1, pp. 370–378, Jan. 2012.
[31] X. D. Xue, K. W. E. Cheng, and S. L. Ho, "Optimization and evaluation of torque-sharing functions for torque ripple minimization in switched reluctance motor drives," *IEEE Trans. Power Electron.*, vol. 24, no. 9, pp. 2076–2090, Sep. 2009.
[32] Y. Jin, B. Bilgin, and A. Emadi, "An offline torque sharing function for torque ripple reduction in switched reluctance motor drives," *IEEE Trans. Energy Convers.*, vol. 30, no. 2, pp. 726–735, Jun. 2015.
[33] T. Weng and C. Pollock, "Two phase switched reluctance drive with voltage doubler and low dc link capacitance," in *Proc. 14th IAS Annu. Meet. Conf. Rec. Ind. Appl. Conf.*, 2005, vol. 3, pp. 2155–2159.
[34] W. Cai and F. Yi, "An integrated multi-port power converter with small capacitance requirement for switched reluctance motor drive," *IEEE Trans. Power Electron.*, vol. 31, no. 2, pp. 3016–3026, Apr. 2016.
[35] B. Fahimi, G. Suresh, J. Mahdavi, and M. Ehsami, "A new approach to model switched reluctance motor drive application to dynamic performance prediction, control and design," in *Proc. IEEE 29th Annu. Power Electron. Spec. Conf.*, 1998, vol. 2, pp. 2097–2102.
[36] S. Hara, Y. Yamamoto, T. Omata, and M. Nakano, "Repetitive control system: A new type servo system for periodic exogenous signals," *IEEE Trans. Automat. Control*, vol. 33, no. 7, pp. 659–668, Jul. 1988.
[37] H. Fujimoto and T. Takemura, "High-precision control of ball-screw-driven stage based on repetitive control using n-times learning filter," *IEEE Trans. Ind. Electron.*, vol. 61, no. 7, pp. 3694–3703, Jul. 2014.
[38] J. H. She, M. Wu, Y. H. Lan, and Y. He, "Simultaneous optimisation of the low-pass filter and state-feedback controller in a robust repetitive-control system," *IET Control Theory & Appl.*, vol. 4, pp. 1366–1376, 2010.

Fan Yi (S'14) received the B.S. degree in electrical engineering from Shandong University, Jinan, China, in 2013. He is currently working toward the Ph.D. degree at the University of Texas at Dallas, Richardson, TX, USA.

He is also a Graduate Research Assistant and Thrust Area Leader in the Renewable Energy and Vehicular Technology laboratory. His research interests include design and control of power electronic converters with applications in renewable energy systems and motor drives.

Wen Cai (S'12) received the B.S. and M.S. degrees in electrical engineering from the Huazhong University of Science and Technology (HUST), Wuhan, China, in 2010 and 2013, respectively. He is currently working toward the Ph.D. degree in University of Texas at Dallas, Richardson, TX, USA.

He is also a Graduate Research Assistant in Renewable Energy and Vehicular Technology Laboratory. From 2009 to 2012, he acted as the Director in HUST-Infineon Joint Training Lab. Since 2012, he becomes a Reviewer for seven journals and several conferences. His research interests include renewable energy applications, multiport converter, resonant converter, switched reluctance motor drives, and power quality optimization of dc microgrid.